UDK 669.14.018.298:621.791:621.785
Pregledni članek/Review article

ISSN 1580-2949
MTAEC9, 44(3)105(2010)

PHYSICAL SIMULATION OF METALLURGICAL PROCESSES

FIZIKALNA SIMULACIJA METALURŠKIH PROCESOV

Stan T. Mandziej

Advanced Materials Analysis, P. O. Box 3751, NL–7500DT Enschede, Nederland
stanamanl@cs.com

Prejem rokopisa – received: 2009-11-16; sprejem za objavo – accepted for publication: 2009-12-08

Worldwide demand of better and more efficient metallurgical processes, leading to low costs of their products, stimulates intensive research to reach these goals. In this respect, any full-scale industrial experiments appear non-acceptable. Cutting off the R&D costs and fast introducing of new technologies is possible when physical and numerical simulations are used. The computer simulation can be only correct when exact data of materials behaviour at processing conditions are known. To obtain the data, physical simulation is needed and it must be executed on multi-purpose thermal-mechanical testing devices accurately reproducing the real industrial processing conditions. For continuous casting or metal forming, individual phases of processes or multi-step operations must be followed, characterized by their time, temperature, and by applied forces, strains and strain rates. Actually the physical simulation, as compared with full-scale industrial testing, allows in a fraction of time for a fraction of cost an improvement of existing technology or development of a new one for modern materials and products. It can be used for solving production problems due to solidification phenomena or deformability limits, which result in hot cracking and rejection of the product. In this paper several examples of physically simulated procedures are given and their physical background discussed.

Key words: physical simulation, Gleeble thermal simulator, deformation, hot cracking, welding, casting

Rast zahtev po boljših in bolj učinkovitih metalurških procesih stimulira po vsem svetu intenzivne raziskave, kako doseči te cilje, ker so za tak namen nesprejemljivi realni industrijski poizkusi. Zmanjšanje RR-stroškov in hitro uvedbo novih tehnologij dosežemo, če uporabimo fizikalno in numerično simulacijo procesov. Računalniška simulacija je natančna, če uporablja prave podatke o vedenju materiala v procesnih razmerah. Da bi te podatke pridobili, je potrebna fizikalna simulacija, ki se izvrši na večnamenski termomehanični preizkusni napravi, ki natančno reproducira pogoje realnega industrijskega procesiranja. Za neprekinjeno litje in oblikovanje kovin je treba upoštevati različne faze procesov, ki se odvijajo v več stopnjah, ki jih karakterizirajo čas, temperatura in uporabljene sile, deformacije in hitrosti deformacije. Fizikalna simulacija, če jo primerjamo z industrijskim preizkusom v polnem obsegu, omogoči, da se v delcu časa za del stroškov doseže izboljšanje sedanje tehnologije ali razvoj nove za moderne materiale in proizvode. Uporabljamo jo lahko za rešitev proizvodnih problemov povezanih s strjevalnimi pojavi ali z mejnimi deformacijami, ki povzročijo vročo pokljivost in izmeček proizvodov. V tem članku predstavljamo primere fizikalno simuliranih procedur in razpravljamo o njihovem fizikalnem ozadju.

Ključne besede: fizikalna simulacija, Gleeblejev termični simulator, deformacija, vroča pokljivost, varjenje, litje

1 INTRODUCTION – PHYSICAL SIMULATION OF WELDING

Historically, welding was the first metallurgical process successfully studied by the simulation technique, in particular the use of simulated thermal cycles to reproduce the situation occurring in parent plate material affected by heat generated during welding. Further development of this technique led to the introduction of several testing procedures aiming to exactly replicate various situations in the weld metal or between the welded joint and adjacent material, in particular these occurring due to the stress relaxation and plastic accommodation processes during multiple heat cycling characteristic of multi-pass welds. The necessity to apply physical simulation for studying ductility and fracture behaviour of heat-affected zones of welds, occurred just after WW-II and was associated with low ductility of the weld heat-affected zone in high-strength steels introduced to shipbuilding [1]. In 1949 the first weld thermal-cycle simulator was built and utilized to generate uniform heat-affected zone microstructures through the CVN-sample for impact testing [2]. At that time, using the simulation, the results of impact strength appeared to be often better than on real welds. This discrepancy initiated more detailed studies on physical phenomena standing behind the toughness of weldments, which studies revealed the role of thermal gradients in affecting phase transformations and generating crystallographic lattice defects to plastically accommodate various micro-strains. Accordingly, the weld thermal-cycle simulator was equipped with a mechanical system capable to deform specimens with adequate speed at exact temperatures. When this was done, the Gleeble thermal-mechanical simulator was born [3]. Since 1957, when the first commercial Gleeble was produced for the purpose of weldability studies, it underwent several metamorphoses and the recent dynamic thermal-mechanical simulators allow the use of physical simulation techniques not only for welding but also for other industrial application processes, such as high strain rate multi-step hot forming with all kinds of thermal-mechanical processes, melting and controlled solidification for the purpose of conventional and continuous casting as well as semi-solid processing, checking for susceptibility

to hot cracking and embrittling, studying sintering, stress relaxation, accelerated creep, thermal-mechanical fatigue, and others.

The main concept of the thermal-mechanical simulator, however, has not been changed much since the beginning, and the actual Gleeble system [4] comprises: an AC electric resistance heating system as it was originally, a mechanical deformation system which earlier was pneumatic and now is servo-hydraulic, a vacuum and/or controlled atmosphere working chamber, and like in all the most recent testing equipments the computer control plus data acquisition and processing. For specific applications it may comprise various working units and attachments. And like at the beginning, the main aim of the physical simulation is to exactly reproduce the thermal and mechanical situation of the workpiece material as it appears in real processing, and to obtain identical microstructures as well as mechanical properties of the physically simulated materials.

1.1 Weld heat-affected zone

In the historical case of welding and its vulnerable to embrittlement and cracking heat-affected zone (HAZ), during the electric arc action a short thermal cycle appeared comprising a rapid heating, followed after reaching peak temperature by a cooling due to heat flow from the hot zone of the weld towards the cooler bulk of the material. The heating and cooling rates result from the balance between the energy input and the heat flow, and are controlled by thermal gradients between the hot zone of the weld and the parent plate. During the thermal cycle the electric current flows through the HAZ and the heat flows from the fusion surface between the weld and the plate to form isothermal planes perpendicular to this main direction of the heat flow, as schematically presented in **Figure 1**. This situation has to be reproduced on a bar-like sample in which a narrow uniformly heated zone is formed in the middle due to the thermal balance between the electric heating and the heat flow towards cold copper jaws, producing real temperature gradients, **Figure 2**. During the weld thermal cycle, a part of the HAZ material at first expands on heating and during this is compressed being restrained crosswise by the cold portions of the parent material, while in the second portion of this cycle the faster cooling down portions of thermal gradient zones once again compress it. In this second part of the thermal cycle also tensile strains appear, in particular in the main direction of the

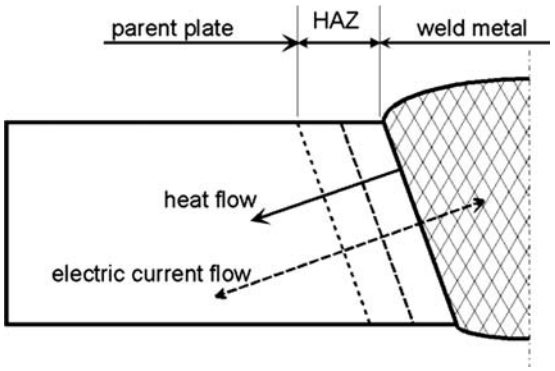

Figure 1: Schematic situation of the heat-affected zone in an arc weld with electric current flow and heat flow.

Slika 1: Shema položaja zone toplotnega vpliva pri elektroobločnem varjenju s smerjo toka toplote

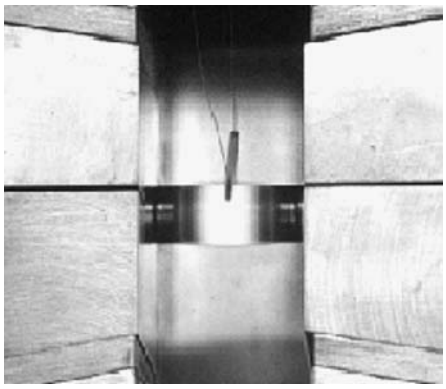

Figure 2: Weld HAZ simulation in Gleeble on 10mm diameter round-bar sample mounted in "cold" copper jaws.

Slika 2: Simulacija v Gleeblejevi napravi za toplotno zono zvara 10 mm na okrogli palici, pritrjeni v hladnih bakrenih čeljustih

a)

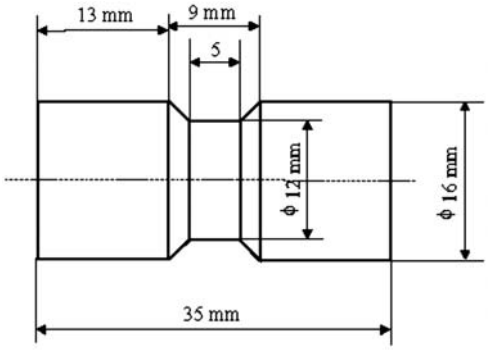

b)

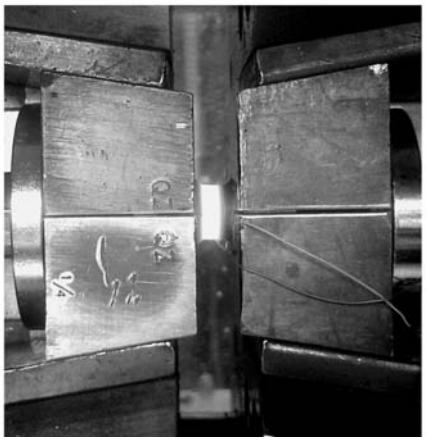

Figure 3: Schematic drawing of Gleeble sample for laser dilatometer studies of phase transformations in steels with cooling rates up to 200 °C/s (a) and this sample mounted in Gleeble's "cold" Cu jaws (b)

Slika 3: Shematična oblika Gleeblejevega preizkušanca za laserki dilatometrski študij faznih transformacij v jeklu s hitrostjo do 200 °C/s (a) in preizkušanec pritrjen v Gleeblejevih hladnih bakrenih čeljustih (b)

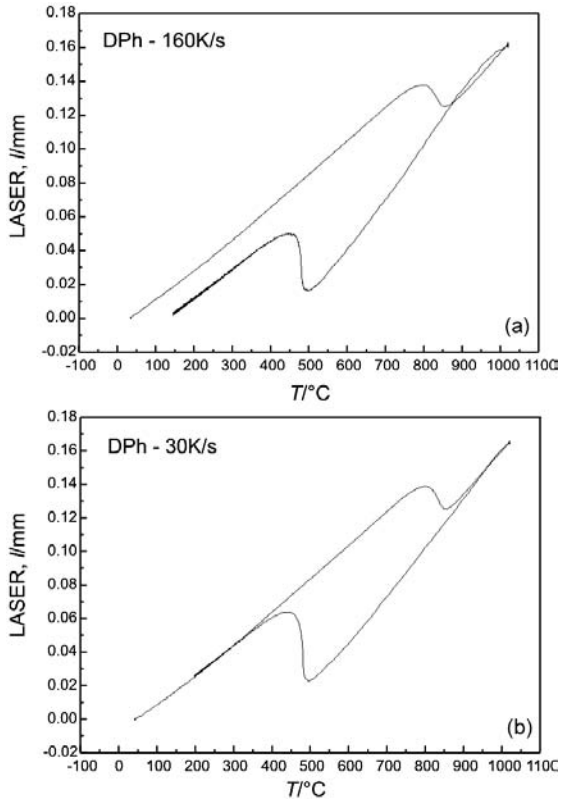

Figure 4: Laser dilatometer curves of HSLA steel heated up in Gleeble to 1020 °C and cooled by heat flow to Cu jaws with rate of 160 °C/s (a) and with rate of 30 °C/s (b).

Slika 4: Laserke dilatometrske krivulje jekla HSLA, ki je bilo v Gleeblejevi napravi segreto na 1020 °C in ohlajeno s pretokom toplote v čeljusti s hitrostjo 160 °C/s (a) in s 30 °C/s (b)

heat flow, and these may assist embrittlement due to generation of dislocations and interaction of these with interstitials [4], or even initiate intergranular cracking.

The magnitude of crosswise deformation due to thermal gradient, which in the case of a stiff real component may result in substantial residual stresses, can be illustrated in the following test. On the sample like in **Figure 3**, tested for phase transformations by contactless laser dilatometer, at the cooling rate of 160 °C/s obtained in the hot gauge zone by heat transfer to cooler mounting portions of the sample fixed in cold copper jaws of the Gleeble, a permanent shrinkage of diameter occurs after the thermal cycle, **Figure 3**. At lower cooling rates of 30 °C/s and less, which produce weaker temperature gradients, such permanent change of sample's diameter may be negligible, **Figure 4**.

1.2 Stress-relief embrittlement

An important demand for the successful physical simulation is its practical accuracy. Certain physical phenomena cannot be detected or studied on samples of wrong size or improper geometry, and then the sensitivity of the testing system must be adequate. Moreover, the physical background of the studied phenomenon must be well known, to properly design the experiment.

Here an example is given from a study on stress-relief embrittlement, occurring in some micro-alloyed HSLA steels and weld metals after post-weld heat-treatment. The stress relieving PWHT carried out at 600 °C converts prior fully acicular ferrite microstructure of the HSLA weld to partly recrystallised one, **Figure 5**, which is brittle and fractures in an intercrystalline mode along columnar crystals of the weld metal, **Figure 6**. This stress-relief embrittlement was associated with initial configuration of crisscrossing $a/2<111>$ screw dislocations, **Figure 7**, dominating in ferrite grains along the boundaries of prior columnar grains, and interaction of these dislocations with interstitials to form meta-stable $a<001>$ edge dislocations [5]. The saturated by interstitials $a<001>$ edge dislocations are mobile and able to enter the columnar grain boundaries to deposit there the interstitials, thus sensitizing these boundaries. An example of such boundary is given in **Figure 8**. Non-embrittling HSLA weld metals of very similar chemical compositions had another initial dislocation substructure and during the stress-relief annealing mainly generated large amount of tangled $a/2<111>$ edge type accommodation dislocations.

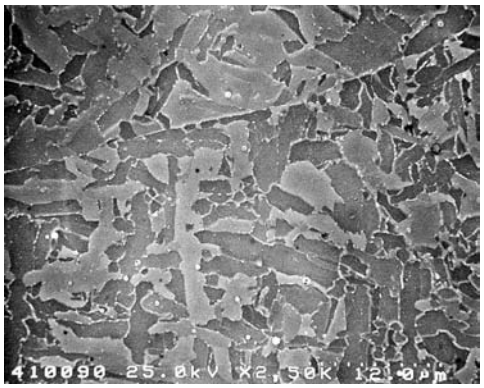

Figure 5: Microstructure of transformed acicular ferrite of HSLA weld metal, showing grain boundary of prior columnar crystals

Slika 5: Mikrostruktura iz transformiranega acikularnega ferita v zvaru jekla HSLA, ki prikazuje meje primarnih stebrastih kristalnih zrn

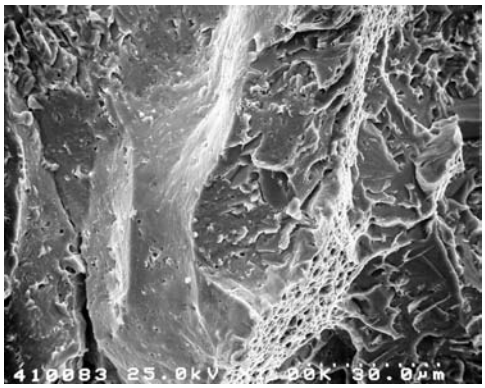

Figure 6: Brittle intergranular and transgranular fracture surface of the stress-relief annealed HSLA weld metal

Slika 6: Krhka intergranularna in transgranularna prelomna površina v napetostno žarjenem zvaru HSLA-jekla

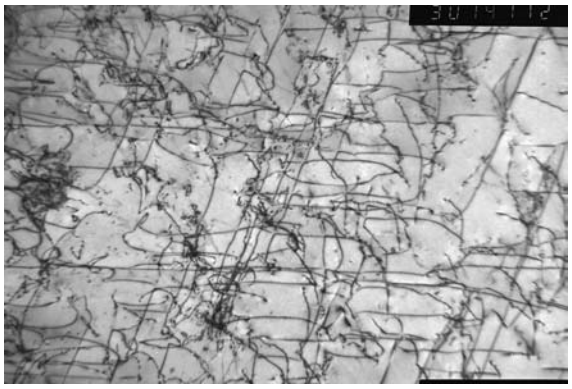

Figure 7: Configuration of criss-crossing screw dislocations dominating in ferrite of the stress-relief embrittling weld metal
Slika 7: Konfiguracija križajočih se vijačnih dislokacij, ki prevladujejo v feritu v zvaru, občutljivem za popustno krhkost

Testing on Gleeble for susceptibility to stress-relief embrittlement comprises 3-step thermal cycling applied on bulk samples of 10 mm to 12 mm diameter, while recording diameter by crosswise contactless laser dilatometer; the setup of this test is schematically shown in **Figure 9**. The laser dilatometer readouts from austenitic stainless steel sample show no changes of its dimensions during such thermal cycling, **Figure 10**.

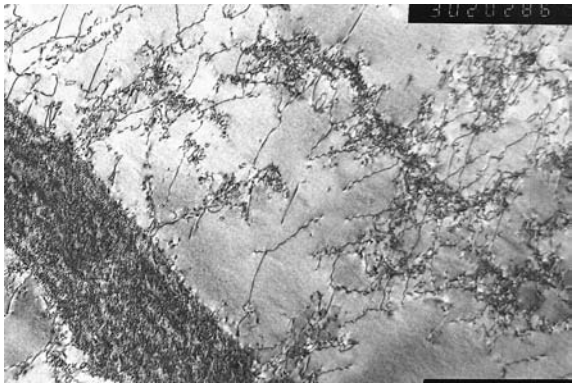

Figure 8: Sensitized grain boundary containing high density of dislocations and fine precipitates in embrittled HSLA weld metal
Slika 8: Sensitivirana krstalna meja z veliko gostoto dislokacij in majhnih izločkov v krhkem zvaru HSLA-jekla

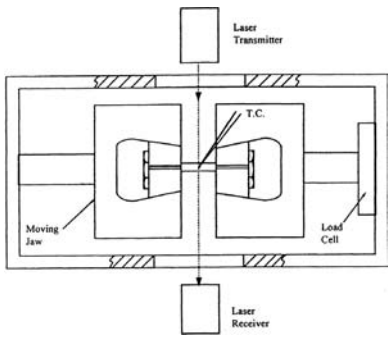

Figure 9: Schematic of laser dilatometer measurement on sample mounted in Gleeble
Slika 9: Shema meritve z laserskim dilatometrom za vzorec v Gleeblejevi napravi

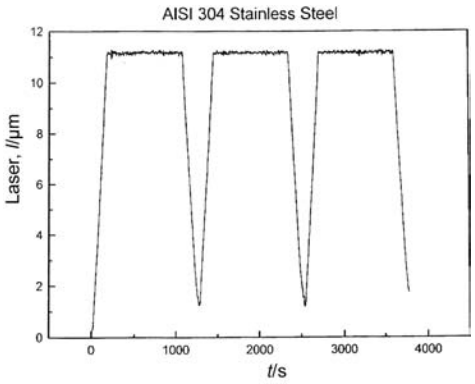

Figure 10: Result of laser measurement during 3-step thermal cycling of austenitic stainless steel
Slika 10: Rezultati meritev z laserskim dilatometrom pri termičnem cikliranju avstenitnega nerjavnega jekla v treh korakih

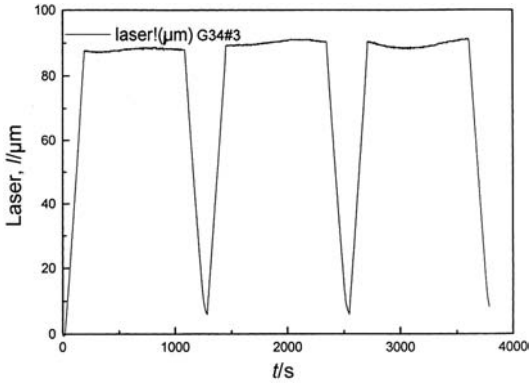

Figure 11: Laser measurement during thermal cycling of non-embrittling HSLA weld metal
Slika 11: Laserske meritve med termičnim cikliranjem zvara HSLA-jekla brez pojava krhkosti

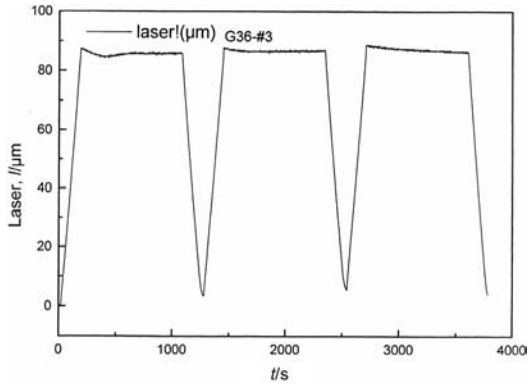

Figure 12: Laser measurement during thermal cycling of embrittling HSLA weld metal
Slika 12: Laserske meritve med termičnim cikliranjem zvara HSLA-jekla z pojavom krhkosti

Samples of a non-embrittling HSLA weld metals during the hold periods of thermal cycles show increase of diameter, **Figure 11**, due to mainly generation of accommodation dislocations, while the embrittling HSLA weld metals in the first cycle show tempering of acicular ferrite (bainite) and in further cycles a steady

decrease of diameter, **Figure12**, associated with reaction of *a*/2<111> screw dislocations into the meta-stable *a*<001> edge dislocations (decrease of density by the factor of ≈2.4) followed by annihilation of the last, mostly within the grain boundaries.

1.3 Hot ductility and hot cracking

One of the main problems of weldability is the susceptibility of some welds to hot cracking, as welding is the technology of joining materials by bringing them locally to the molten state and then solidifying this region. At high temperatures just below solidus most of metal alloys suffer loss of strength and ductility. This occurs on heating due to liquation before reaching the fully molten state and then on cooling from the melt it persists within certain range of temperatures after solidification, called brittle temperature range – BTR. As the solidified alloy becomes stiff while not yet ductile, hot cracks may form on cooling, when tensile strains caused by shrinkage and assisted by restraint cannot be compensated by ductility of this alloy. Accordingly, the method of studying susceptibility of an alloy to hot cracking involves tensile testing at the conditions simulating these of the real welding (or casting) process. The use of thermal-mechanical simulator like Gleeble, able to reproduce on a specimen the welding thermal cycle and impose a strain in a controlled manner, allows achieving this goal.

Hot tensile test

Testing on Gleeble for susceptibility to weld liquation cracking / HAZ hot cracking, is the hot tensile testing of a number of specimens on-heating and then on-cooling, and determining their hot ductility measured as a reduction in area at the specimen's neck portion after the test. This procedure is schematically presented in **Figure 13** [6].

The hot ductility of a welded alloy increases gradually with increase of testing temperature from ambient towards melting point, however, before reaching this point it drops abruptly from certain maximum to nil. Just above this nil ductility temperature (NDT) is the nil strength temperature (NST) at which the alloy looses its strength due to liquation i.e. formation of weak or liquid phases along grain boundaries. The real physically measurable melting temperature of such alloy – TL, is higher than NST. On-cooling from the melt or from the NST, the ductility does not recover exactly at NDT only below it at so-called ductility recovery temperature – DRT. The temperature span from NST to DRT is considered to be the brittle temperature range – BTR, the extent of which can be used as a rough criterion of the susceptibility to hot cracking.

More exact criterion of this susceptibility is the measure how fast does the ductility recover on-cooling as compared with its decrease on-heating. As reference point for this measurement the maximum of ductility from the on-heating ductility curve is taken and the representative areas below the on-heating and on-cooling curves are compared, **Figure 14** [7]. Arbitrarily considering 5 % of reduction-in-area on-cooling as the ductility recovery point and comparing the hot ductility curves on-heating and on-cooling, the nil ductility range (NDR), ductility recovery rate (DRR) and ratio of ductility recovery (RDR) can be determined to exactly characterize the susceptibility of an alloy to hot cracking.

The reference point for the hot ductility measurements determining the susceptibility to liquation cracking is the nil strength temperature. This temperature has to be used as a peak of the welding thermal cycle, on-cooling after which the hot tensile tests should be run. To measure the NST on Gleeble an attachment is used, schematically presented in **Figure 15**. This NST attachment keeps the specimen under a constant tensile load of about 50 N while allowing its heating-up with an initial heating rate the same as of the welding thermal cycle to be simulated up to a temperature 50 °C below the solidus temperature of the material, then change to a heating rate of 2–5 °C/s until the NST is reached, as shown in **Figure 16**.

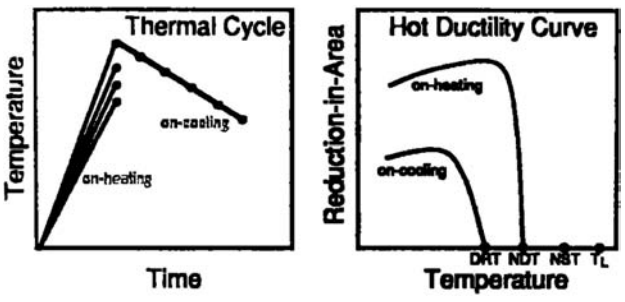

Figure13: Schematic of Gleeble's procedure for hot cracking, including hot tensile testing on-heating up to NST and then on-cooling after weld thermal cycle with NST as the peak temperature [6]

Slika 13: Shema Gleeblejeve procedure za vročo pokljivost, ki obsega vroč raztržni preizkus s segrevanjem do NST in ohlajanje po termičnem ciklu varjenja z NST kot najvišjo temperaturo [6]

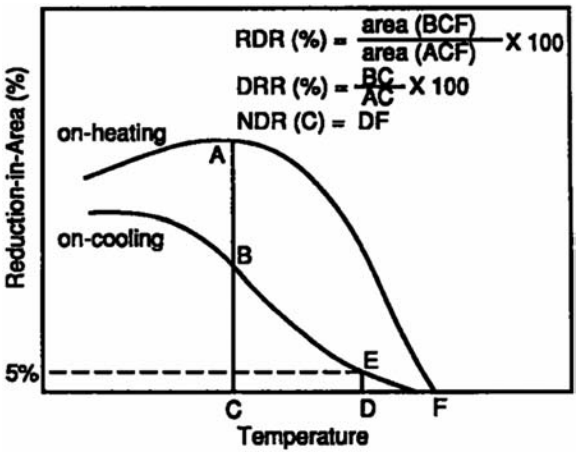

Figure 14: Evaluation of hot ductility curves for the hot cracking susceptibility [7]

Slika 14: Ocena krivulj vroče duktilnosti za občutljivost za vročo pokljivost [7]

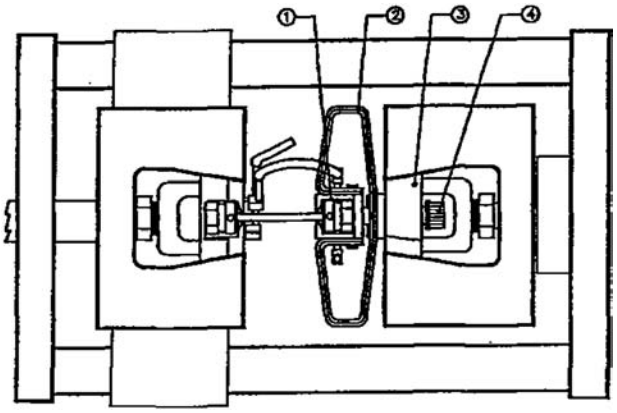

Figure 15: Nil strength attachment of Gleeble using trapezoidal spring grip maintaining constant small tensile load on specimen during heating

Slika 15: Shema montaže brez sile v Gleeblejevo napravo s prijemom z uporabo trapezoidalne vzmeti, ki ohranja konstantno majhno natezno napetost med ogrevanjem preizkušanca

To avoid mixing-up of phenomena related to liquation cracking with these of solidification cracking, in order to measure only the hot ductility region responsible for the liquation cracking, the NST must not be exceeded in the simulated weld thermal cycles.

To test for the susceptibility to solidification cracking, controlled melting and solidification of a rod-like specimen can be carried out on Gleeble, and after the solidification the hot ductility is determined in the manner like described above. Here the ability of Gleeble to melt electrically conductive specimens is used. In this test the central portion of the specimen protected by a crucible / quartz sleeve is brought to a temperature above solidus and then this crucible contains the molten / semi-liquid metal, as shown in **Figure 17**. Thermal gradients between the molten portion and mounting jaws prevent the metal from flowing out of the crucible while controlled thermal cycle allows conducting the solidification in a manner similar to that of

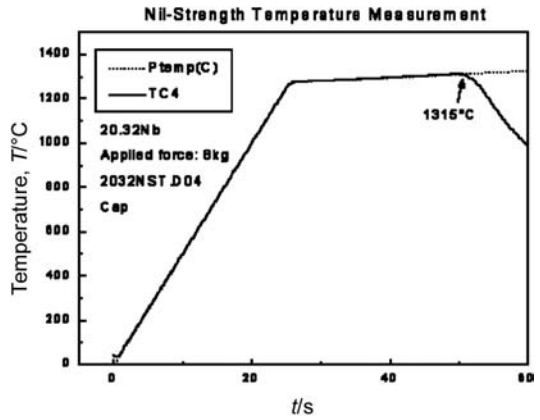

Figure 16: Time – temperature graph of Gleeble test for nil strength temperature

Slika 16: Graf čas – temperatura Gleeblejevega preizkusa za temperaturo ničelne trdnosti

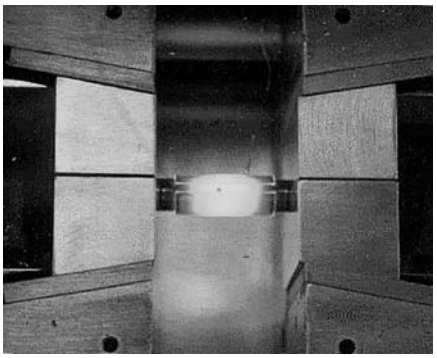

Figure 17: Gleeble's setup for controlled melting and solidification study

Slika 17: Gleeble postavitev za raziskave kontroliranega taljenja in strjevanja

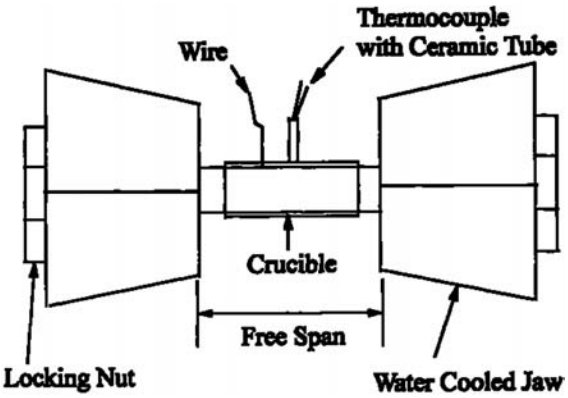

Figure 18: Schematic of **Figure 17**, with end nuts for hot tensile testing

Slika 18: Shema **slike 17** s končnimi vijaki za vroč natezni preizkus

real casting or welding. Schematic of the assembly used for this purpose in Gleeble is given in **Figure 18**.

More details of the Gleeble testing for liquation and solidification cracking can be found in IIW document No. II-C-042A/95 [8]. The Gleeble testing procedures are also mentioned in the technical report CEN ISO/TR 17641-3:2003, under the chapter "Hot Tensile Test" [9].

The SICO test

An alternative procedure to study susceptibility to solidification cracking on Gleeble is the strain-induced crack opening test – SICO, developed at Dynamic Systems Inc., in USA, for studying hot deformability of alloys. In this test the central hot portion of the Gleeble specimen is compressed to form a bulge, **Figure 19**, on outer perimeter of which cracks appear at the critical secondary tensile strain, **Figure 20**. The critical strain to fracture in SICO test is defined as the hoop strain at onset of cracking in the bulge zone:

$$\varepsilon_c = \ln (D_f/D_o)$$

where D_o is the initial diameter of the specimen, while D_f is the final maximum diameter in the bulge zone.

As during the controlled melting and solidification in Gleeble the dendritic crystals mostly grow from the direction of the main heat flow i.e. in the axial direction,

Figure 19: SICO sample tested in Gleeble
Slika 19: SICO-preizkušanec med preizkusom na Gleeblejevi napravi

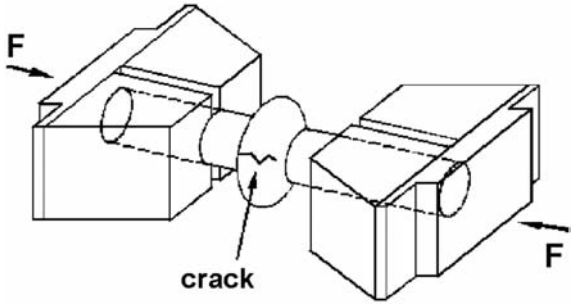

Figure 20: Schematic of SICO test showing crack formed on bulge portion of sample
Slika 20: Shema SICO preizkusa z napako na izbočenem delu preizkušanca

the mid-span segregation may occur in the specimen causing deep and partly hidden cracking of the SICO specimen along the central plane perpendicular to the compression axis, **Figure 21**. In such situation it is advised to check for the true critical diameter on the cross-section of SICO sample, like it is shown in **Figure 22**.

As the hot tensile testing on Gleeble gives the adequate characteristics of an alloy regarding its hot cracking susceptibility, the SICO test appears to be more accurate for measuring of critical strains to fracture and related critical strain rates.

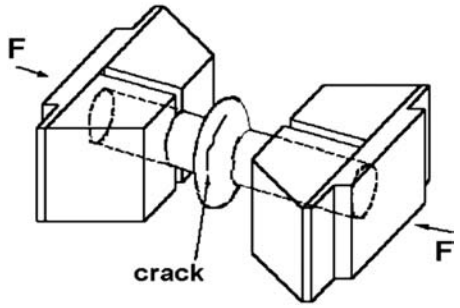

Figure 21: Central plane crack in SICO often appearing after melting and solidification
Slika 21: Razpoka v centralni ravnini na SICO-preizkušancu, ki pogosto nastane po taljenju in strjevanju

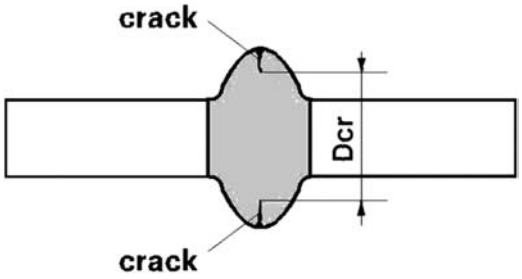

Figure 22: Method of measuring critical diameter *D*cr when central plane crack appears
Slika 22: Metoda za merjenje kritičnega premera *D*cr v primeru razpoke v centralni ravnini

2 SIMULATION OF CASTING

The physical simulation actually plays an important role in the design and application of the most efficient industrial manufacturing process, which is the continuous casting and the hot rolling following it. As shown in **Figure 23**, in different stages of process may occur flaws such as shrinkage cavity, centre-line porosity, facial and corner cracks [10]. Physical simulation can be used to determine flawless processing parameters, without interrupting of production.

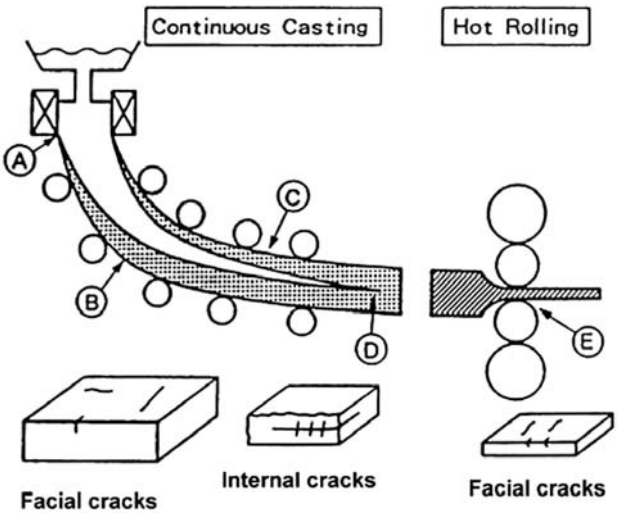

Figure 23: Schematic of continuous casting and hot rolling processes [10]
Slika 23: Shema neprekinjenega litja in vročega valjanja [10]

2.1 Controlled solidification and semi-solid processing

In the first phase of process like schematically shown above, the liquid metal is poured into a crystallizer chamber in which its outer shell has to solidify to the extent securing the liquid core inside. When a vertically cast slab or billet has to be bent into horizontal position, the ductility of outer shell must allow this. Gaining physical data for such operation includes melting and solidifying of numerous samples in the manner like presented in **Figures 17 & 18**, and hot tensile testing

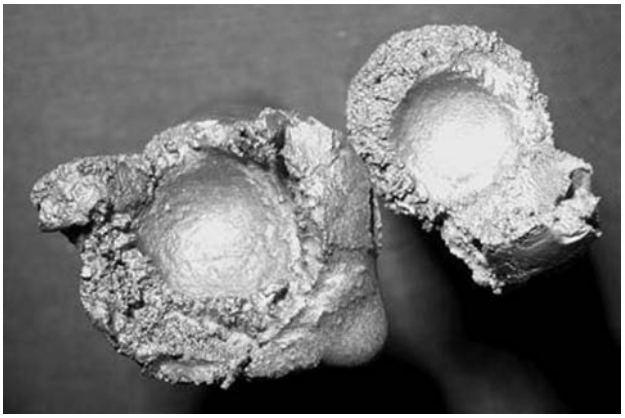

Figure 24: Sizes of solidified outer shell and molten pool in 25 mm SICO bar melted at 1465 °C and then compressed at 1420 °C surface temperature, while the middle temperature being of ≈1450 °C
Slika 24: Velikosti strjene zunanje lupine in talilne kopeli v 25 mm SICO-palici, ki je bila staljena pri 1465 °C in krčena pri temperaturi površine 1420 °C, ko je bila temperatura v sredini ≈1450 °C

them at various temperatures after solidification, to create hot ductility maps [10].

An alternative test comprises melting of a 25 mm diameter bar and deforming it by compression after a partial solidification. The heating-cooling balance of Gleeble causes in the sample thermal gradient to occur keeping molten core inside when outer shell solidifies. The test called 25 mm SICO gives critical strain to fracture, strain rate and temperature, and in the case of incomplete solidification reveals thickness of outer shell on crashed sample, **Figure 24**.

Distribution of strains in the SICO sample can be determined by numerical simulation [11]. Having known the strain distribution and temperature gradient as well, valuable information can be gained from cross section of the sample like given in **Figure 25**: cracks at maximum perimeter occurred at temp of 1385 °C and 0.35 strain with 0.5/s strain rate, then no-crack zone at ≈0.5 of radius appeared representative to temperature ≈1400 °C and strain of 0.2, and once again cracks in the middle of the sample were formed representative to strain ≈0.05 at temperature of ≈1425 °C, the last is the nil ductility temperature of the tested steel.

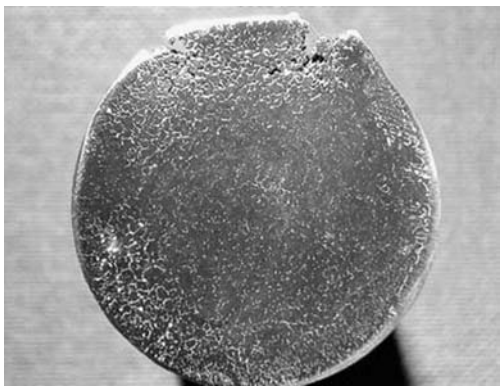

Figure 25: Cross-section of SICO sample showing deep cracks along perimeter and cracks in the middle, with flawless zone in between
Slika 25: Prečni prerez SICO-preizkušanca z globokimi razpokami vzdolž oboda in razpokami v sredini z področjem brez napak med obema

2.2 Direct casting and rolling

The recent development in continuous casting consists of thin strip casting followed directly by hot rolling while retaining the heat of the melt. For simulation of such process the dedicated HDS-V40 physical simulator has been built [4,12], allowing on one specimen after melting and solidification with controlled dendrite size and growth direction to perform multi-step high rate deformations representative to multi-stand rolling. The process comprises resistance heating of a bulk 10 mm thick, 50 mm wide and 165 mm long specimen in a specifically designed crucible, to melt the central portion of this specimen and then to solidify it in a controlled manner, and then to deform its central portion by heated plane strain anvils perpendicularly to the lengthwise axis. Upon melting and subsequent cooling a thin shell forms around the molten material and as soon as it appears the melting crucible is pulled away from the specimen to allow for deformation. Schematic of this process is given in **Figure 26**. Multiple hit deformations by plane strain compression, **Figure 27**, can then be performed on the material while it is in the solid or semi-solid state. Resulting from the simulation is the flat bar, **Figure 28**, with central deformed zone (5), transient zone (4) and side zones of reheated in solid state coarse-grained material (1), mushy zone (2) and fully melted (3) material; in this picture marked by hatching are sections used in subsequent metallographic examination.

The reliability of the melting and solidification procedure can be discussed in terms of non-metallic inclusions before and after the experiment. The specimen made of 0.2 % C plain carbon steel, had in the initial

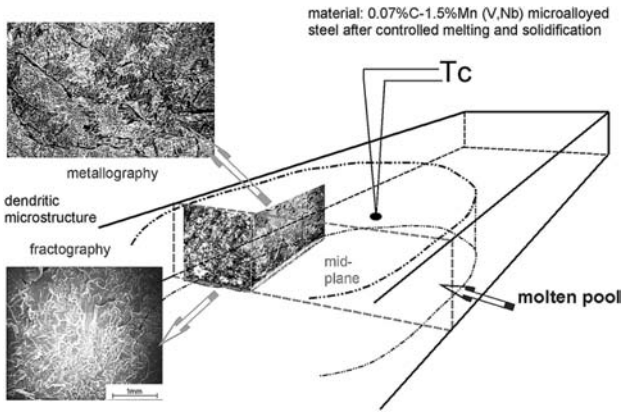

Figure 26: Schematic of the melting and solidification test in HDS-V40 simulator, showing the site and shape of the molten pool and then formed columnar crystals as visible on longitudinal section and on fracture in the mid-plane
Slika 26: Shema talilnega in strjevalnega preizkusa v HDS-V40 simulatorju, ki kaže mesto in obliko staljene kopeli in nato nastalih stebrastih zrn, kot se vidijo na vzdolžnem prerezu in na prelomu v srednji ravnini

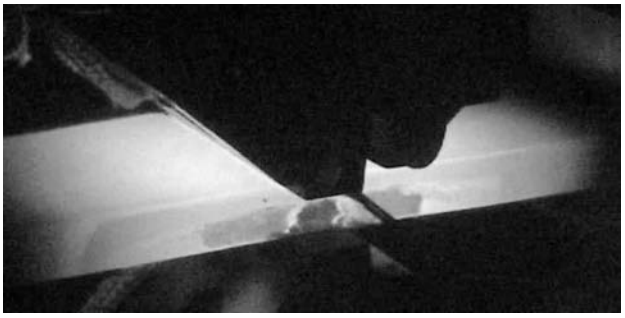

Figure 27: Hot central zone of specimen and plane strain anvils in the working chamber
Slika 27: Vroča centralna zona preizkušanca in čeljusti za napenjanje v delovni komori

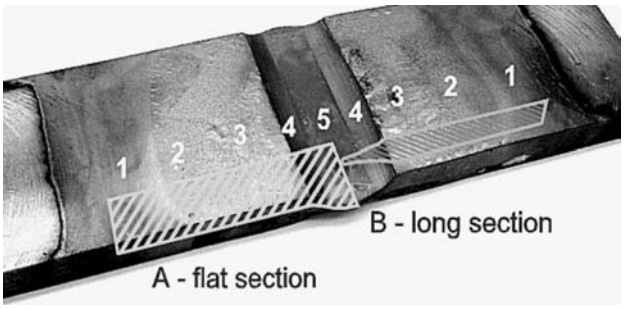

Figure 28: Specimen after simulation of melting and direct hot rolling
Slika 28: Preizkušanec po simulaciji taljenja in direktnega vročega valjanja

state a ferritic-pearlitic microstructure with bands elongated in rolling direction and so extended non-metallic inclusions. After the test, in the entirely melted and solidified "as-cast" zone-3, chains of spheroidal inclusions dominated along boundaries of dendrites, **Figure 29**. On fracture through mid-plane of the as-solidified specimen, which coincides with the mid-plane of the former molten pool, individual dendritic crystals are seen, **Figure 30**, with their lengths of up to 2.0 mm. This size of dendrites

Figure 30: Cleavage fracture along mid-plane of specimen, showing sizes of dendritic crystals
Slika 30: Cepilni prelom vzdolž centralne ravnine preizkušanca, na katerem vidimo velikost dendritnih zrn

Figure 29: Fine spheroidal inclusions in grain boundary ferrite of dendritic crystals
Slika 29: Fini sferični vključki v feritu po kristalnih mejah dendritnih zrn

well coincides with the length and width of dendritic crystals appearing in the thin continuously cast slabs manufactured in the industrial processes [13].

3 SIMULATION OF HOT DEFORMATION

Two major hot deformation procedures: forging and rolling, have to be physically simulated in a different manner, due to differences in main force direction, main strain direction and heat flow, as schematically given in **Figure 31**. Thus to simulate forging an axial compression / flow stress test is used, while for simulation of rolling the plane strain compression has to be applied.

3.1 Multi-step deformation

An exact simulation of multi-step hot rolling by plane strain compression test requires constant strain rates to be maintained in each step with an instantaneous stop at

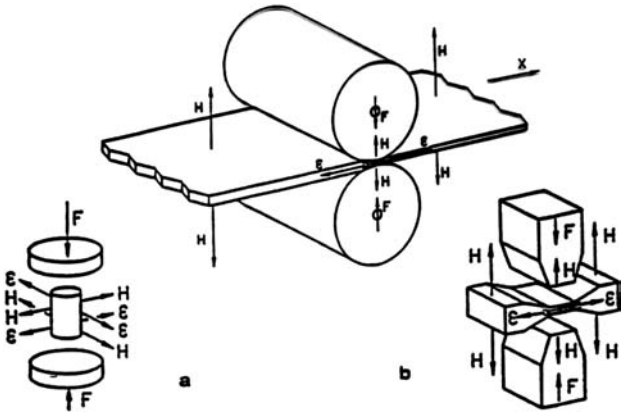

Figure 31: Schematic presentation of a roll stand and simulation of deformation by: (a) flow stress test, and (b) plane strain test. The letters denote: *F* – compression force; *H* – heat flow direction; *ε* – strain direction: *X* – rolling direction [14]
Slika 31: Shema valjalniškega ogrodja in simulacija s: (a) preizkusom meje tečenja in (b) z ravninskim deformacijskim preizkusom. Črke pomenijo: *F* – tlačna sila, *H* – smer toka toplote, *ε*- smer deformacije, *X* – smer valjanja [14]

the end of deformation. To achieve such performance of the Gleeble's servo-hydraulic system, a dedicated deformation-assisting device called Hydrawedge was designed and implemented [14]. The Hydrawedge, synchronized with the main / primary deforming system, is acting as a flexible mechanical stop that allows the primary hydraulic ram to be stopped by running into an immovable object. In order to perform exact multiple compressions sequentially, for which the specimen must be moved since the main hydraulic ram will stop at the same point in space each time, the Hydrawedge is used to program the displacements. This allows to exactly control the amount of strain, while simultaneously and separately controlling the strain rate at which the sample is being deformed. Without such device, all fast servo-hydraulic machines or give substantial over-travel or must slow down before stopping at the right sample's height. In the first instance other than programmed strains are generated while in the last case final microstructures are generated characteristic of slower than programmed strain rates.

In **Figure 32** the schematic of Hydrawedge is given and in **Figure 33** its operation explained. In the system consisting of main power piston (M), punch with stop (P), yoke (Y), sample (S) and Hydrawedge piston (H), before deformation the system is in position like drawn in **Figure33**(a). Preparation to deformation includes pulling off the main piston (M) to form a gap "g" between it and punch (P). Simultaneously the Hydrawedge piston (H) pushes the sample (S) and punch (P) to set-up the amount of required deformation between the punch's stop ring and the yoke (Y), **Figure 33**(b). Finally in the deformation step, **Figure 33**(c), the main piston accelerates through the gap "g" reaching the required top speed, then during the deformation decelerates in a programmed manner to maintain constant strain rate, and when the stop of the punch (P) hits the yoke (Y), the deformation is finished with high accuracy. Such steps can be then repeated several times.

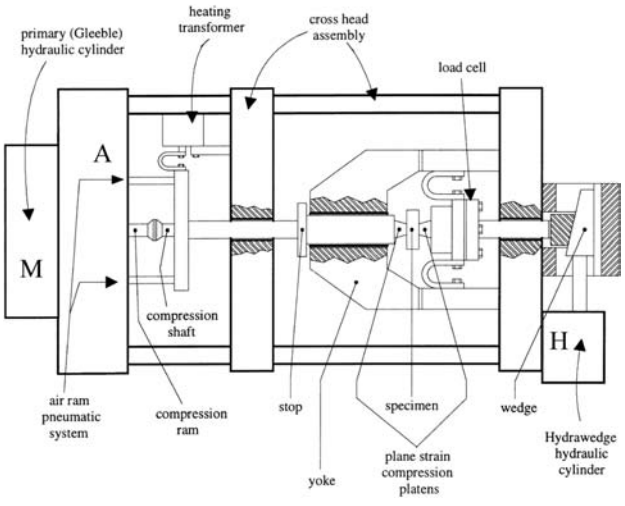

Figure 32: Schematic drawing of the Hydrawedge device [14]
Slika 32: Shema vlečenja na napravi Hydrawedge [14]

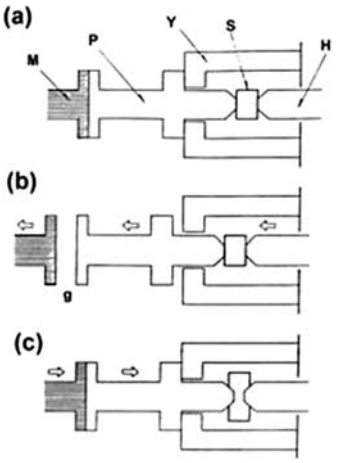

Figure 33: Hydrawedge operation
Slika 33: Preizkus Hydrawedege

Maintaining constant strain rates and instantaneous termination of each deformation step with an aid of Hydrawedge reveals true behaviour of the material under processing. Theoretical deformation behaviour assumes continuous strain hardening and increase of flow stress with decrease of deformation temperature, **Figure 34**. In reality, due to microstructure transformation processes like dynamic and static recrystallisations and precipitations overlapping with these, the true multi-step flow stresses are often much different, **Figure 35**.

An example, which follows, shows how the physical simulation can be used to generate various as-hot-rolled microstructures. A HSLA steel, used for manufacturing of hot rolled plates in a 7-step rolling process, as in **Figure 36**, with continuous drop of temperature, had an acicular ferrite / upper bainite microstructure with very uniform grain size across the plate thickness, given in **Figure 37**. On this steel an attempt was made by physical simulation on Gleeble, to refine grains, separate the phases, achieve a dual-phase microstructure, as well as to reduce amount of deformation steps in the rolling mill.

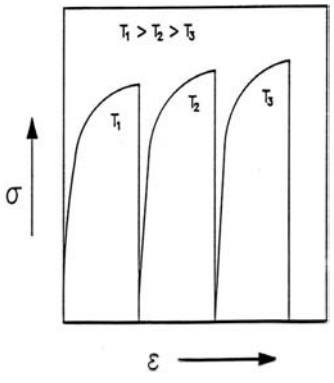

Figure 34: Theoretical flow stress curves of multi-step hot deformation
Slika 34: Teoretične krivulje tečenja pri vroči deformaciji v več stopnjah

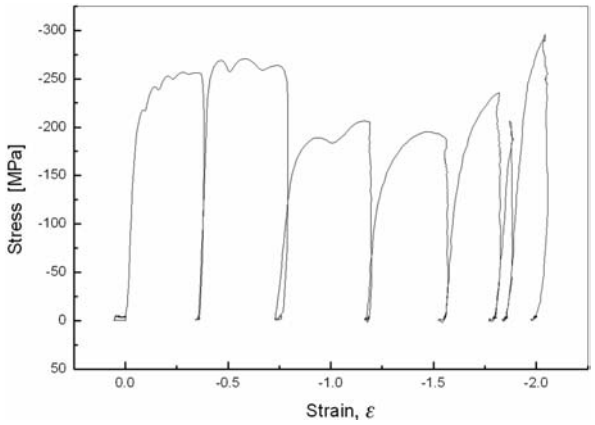

Figure 35: True stress-strain graph of the 7-step hot rolling simulated in Gleeble

Slika 35: Pravi graf napetost – deformacija simulacije valjanja v 7 vtikih v Gleeblejevi napravi

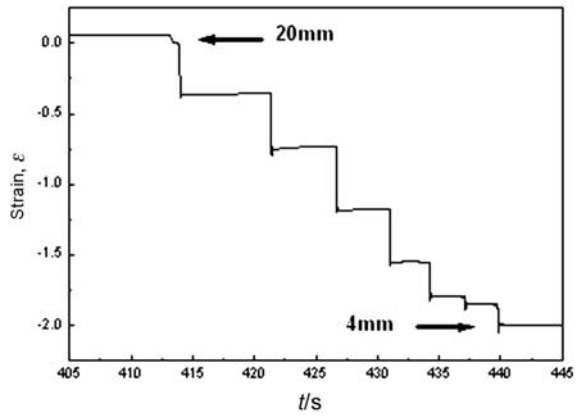

Figure 36: Strain vs. time of the 7-step rolling schedule simulated in Gleeble

Slika 36: Odvisnost deformacije od časa pri simulaciji valjanja v 7 vtikih v Gleeblejevi napravi

One of the methods to obtain the dual-phase microstructure is an intercritical annealing followed by accelerated cooling. An alternative is to stimulate by deformation the phase separation in the two-phase intercritical

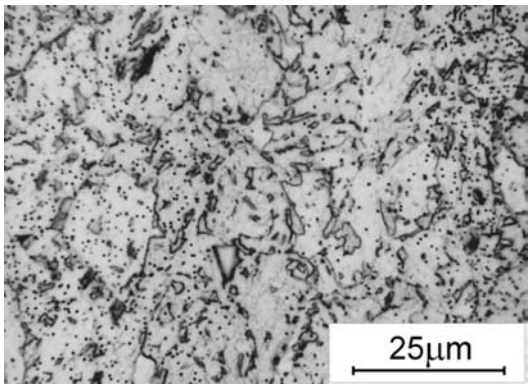

Figure 37: Microstructure of acicular ferrite / bainite with uniform distribution of carbides

Slika 37: Mikrostruktura iz acikularnega ferita/bainita z enakomerno porazdelitvijo karbidov

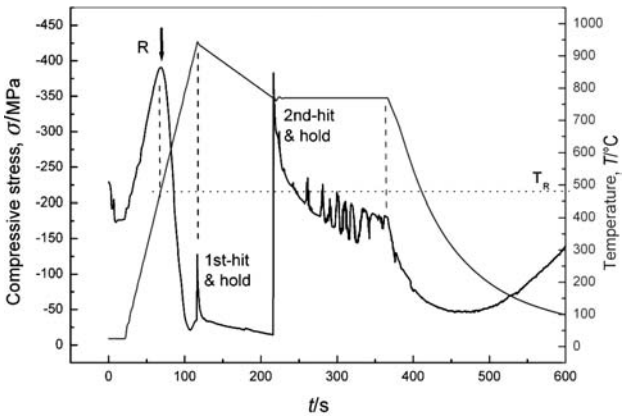

Figure 38: The 2-step deformation and relaxation test in the intercritical range followed by cooling, as simulated in Gleeble

Slika 38: Simulacija v napravi Gleeble za deformacijo v dveh korakih; preizkus relaksacije v interkritičnem področju ter hlajenje

austenite-ferrite range. The new requested continuous 5-step rolling procedure needed a proof that for the selected steel this would be achieved. The appropriate test on Gleeble comprised applying small strains after which the relaxation of sample was monitored. Two- and three-hit experiments were carried out with different time intervals after the hits. An example of a 2-hit experiment is displayed in **Figure 38**. A sample pre-loaded to 175 MPa compression stress at room temperature was heated with constant rate of 10 °C/s to above A_3 temperature in fixed Gleeble jaws, showing relaxation temperature of about 480 °C. After reaching 920 °C it was deformed by the first hit and then held to relax for 100 s while the temperature was constantly dropping. The second hit was executed at 770 °C and during the hold for 150 s after it the austenite-to-ferrite isothermal transformation effects were observed.

Further a free cooling was applied, during which at first the effects were observed of austenite-to-martensite transformation and then "stiffening" of the ferritic-martensitic microstructure.

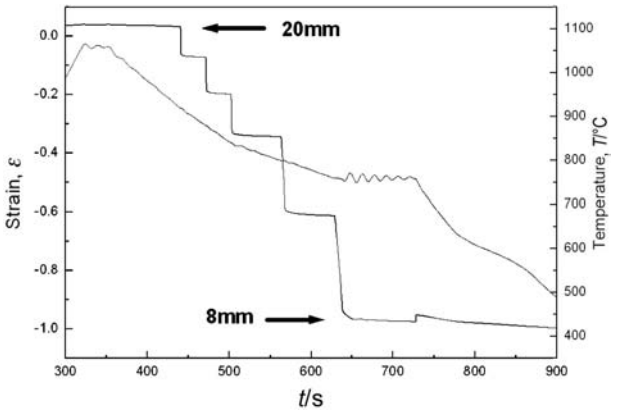

Figure 39: Strain vs. time and temperature profile of 5-step simulation to achieve fine-grained microstructure

Slika 39: Odvisnost napetosti od časa in temperaturni profil pri simulaciji v 5 korakih za dosego finozrnate mikrostrukture

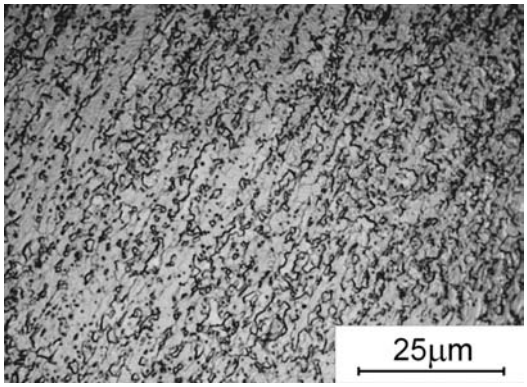

Figure 40: Fine-grained microstructure if the deformation bands after the 5-step rolling simulation in Gleeble

Slika 40: Finozrnata mikrostruktura v deformiranem pasu po simulaciji valjanja v 5 vtikih v Gleeblejevi napravi

The final 5-step rolling procedure, **Figure 39**, comprised three initial steps in austenite phase, maintaining strains, strain rates, as well as interpass times and temperatures adequate to preserve and/or to additionally stimulate precipitation of fine carbides. The last two steps were executed in the austenite-ferrite two-phase region according to the results from tests like this presented in **Figure 38**. The resulting fine-grained microstructure, which on plane strain samples reduced to only ≈1.0 total strain formed mainly in shear-bands, is shown in **Figure 40**. By an increase of strains in all five steps of this new rolling procedure the uniform fine-grained microstructure was obtained across the whole thickness of the plate.

3.2 Solving problems in hot rolling

Flawless rolling process requires that characteristic of the material strains to fracture got never exceeded. In hot deformation tests steeper temperature gradients cause apparent strengthening of the material and decrease of its ductility. In industrial manufacturing this phenomenon is often responsible for appearance of corner cracking of hot rolled billets. The lower temperatures of the corner region always appear, **Figure 41a**, and corner or near-corner cracks may occur when the flow of material to the corner of billet is hampered by the thermal gradients. This situation, schematically given in **Figure 41b**, shows how normal force and friction forces exerted by rolls cause the material flow in the rolling direction as well as towards the corners, while the plasticity of the material along the cooler corners may be limited. Solving of this problem requires hot strength and ductility data that might be provided by numerous hot tensile tests [14].

As an alternative to physically reproduce this situation, a two-step SICO test may be used (**Figure 42**). After forming a bulge in the first compression deformation, an air (or inert gas) blow is locally applied to produce the measured by two thermocouples *T*c1 & *T*c2 thermal gradient like in the real situation, and when this gradient is achieved the second compression is applied, with adequate second strain and proper strain rate, till the

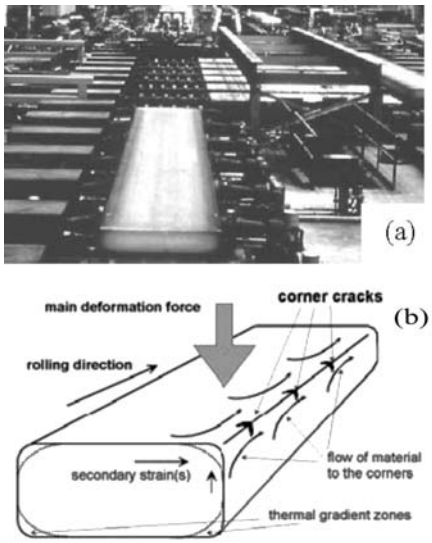

Figure 41: The real situation of hot rolled steel slab (a) with cooler corner portions, and its schematic explanation indicating the directions of main metal flow

Slika 41: Pravo stanje vroče valjanega slaba s (a) hladnejšimi vogali in shematsko označbo smeri glavnega toka metala

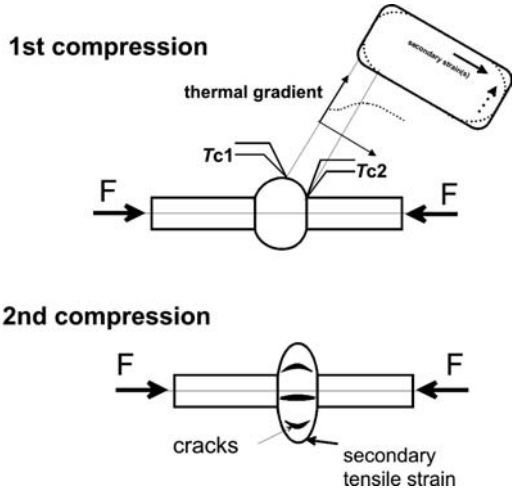

Figure 42: A two-step SICO test for susceptibility of hot rolled billets to corner cracking, including: the first compression to form a bulge, holding till the gradient appears and the final second compression

Slika 42: Dostopenjski SICO- preizkus občutljivosti vroče valjanih slabov za vogalne razpoke, ki obsega: najprej krčenje za nastanek izbokline, zadržanje do nastanka gradienta in nato drugo, končno krčenje

cracks appear. This procedure gives the amount of strain to fracture at the real strain rate, at controlled temperature and at real temperature gradient – it is not easy to gain all these data simultaneously in any other simple and continuous test.

4 THERMAL-MECHANICAL FATIGUE

The thermal-mechanical fatigue is a complex process often responsible for premature failure of components in power generation and chemical processing. In recent four decades microstructural features were identified,

which in novel creep resisting martensitic / ferritic steels accelerate precipitation of carbides and speed-up recovery and recrystallisation of matrix. Based on these evidences a low-cycle thermal-mechanical fatigue procedure called accelerated creep test (ACT) was developed on Gleeble. The ACT speeds-up microstructural changes by elasto-plastic tensile and compressive strains applied on the sample during thermal cycling in the temperatures characteristic of creep. It also uses the advantages of direct electric resistance heating, which is the heating mode implemented on Gleeble and also complies with the recent knowledge on development of dislocation substructures and their effect on precipitation processes in ferritic and multi-phase steels [15].

4.1 The accelerated creep test – ACT

The up to date ACT procedure complies with the following principles:

- The basic temperature and applied strains prevent odd transformations like e.g. secondary dissolution of carbides or intensive formation of non-equilibrium phases.
- The final deformation at fracture is like at real creep – just a few pct in total.
- The depletion of weld metal or steel matrix in alloying elements is achieved similar to that of crept steels and the carbide phases at onset of cracks are not different.

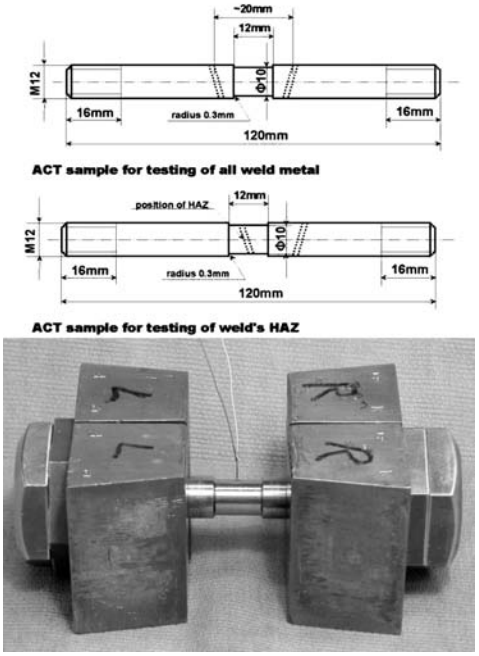

Figure 43: Schematic drawing of cross-weld samples used for ACT on all-weld-metal and on weld's HAZ, and mounting of the sample in Gleeble's jaws set

Slika 43: Shema križnih varilnih preizkušancev za ACT na metalu zvara in coni toplotnega vpliva zvara ter pritrditev preizkušanca v čeljusti Gleeblejeve naprave

Size and mounting of specimens in Gleeble allows a uniformly heated zone formed in the middle-span of the sample and the portion of material in this zone undergoes transformation. To better define this zone, gauge portion of a reduced diameter is made on the sample, **Figure43**.

The ACT was primarily invented for welded joints, in particular for repair welding. Its first larger application appeared in the 5thFP EU R&D project "SmartWeld" (2001–2004) and more recently in COST-536 and COST-538 EU actions.

The ACT samples mounted in the Gleeble's "pocket jaws" assembly, like in **Figure 44**, were subjected to programmed cycles of the low-cycle thermal-mechanical fatigue, run till failure or till pre-determined stress or strain. In homogeneous materials, often before the crack appearance on the surface, internal cracks were formed extending perpendicularly to the sample's axis. In microstructurally inhomogeneous samples the cracks usually followed the "weakest links" like the HAZs of the welds.

4.2 Results of the ACT

In the implemented low-cycle thermal-mechanical fatigue procedure on Gleeble data of stress, strain, strain rate and temperature as well as dilatometric information are recorded, out of which strain-time and stress-time graphs can be produced like these given below in **Figure 45**. Usually the tests are run till failure of specimen, however the test can be interrupted anytime and specimens for e.g. fine fractographic and microanalytical investigations taken before fracturing. As the tests for different materials are run at different temperatures and the response of material gives various stress equivalent to the YS at elevated temperature of the test, to compare the ACT results the duration of the test and its temperature can be included in the following parameter:

$$P_{\mathrm{ACT}} = (7 + \log t) \cdot T/100$$

where: t/ks = time of test, and T/K = temperature.

Then, the creep strength factor in ACT can be calculated as:

$$F_{\mathrm{ACT}} = P_{\mathrm{ACT}} \cdot R_{\mathrm{S}}/100$$

where R_S is the average stress of all ACT cycles measured during relaxation on tension.

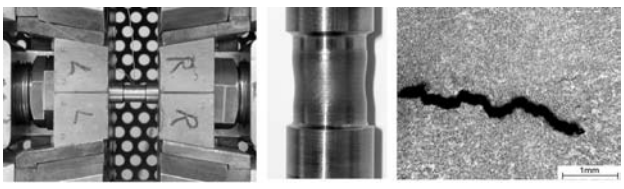

Figure 44: ACT sample located in the Gleeble "pocket jaw" assembly, then shape of the sample after the test and the internal crack formed during the test in the neck portion of this sample

Slika 44: ACT-preizkušanec v žepnih čeljustih Gleeblejeve naprave; oblika preizkušanca po preizkusu in notranja razpoka, nastala v vratu preizkušanca

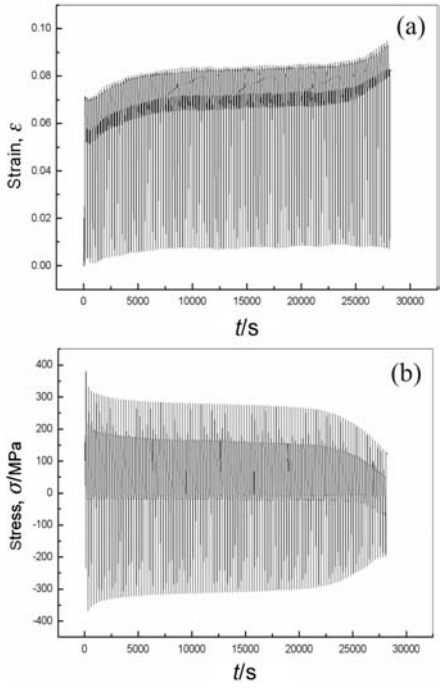

Figure 45: Strain-time (a) and stress-time (b) graphs, from ACT at 600 °C on a post-weld heat-treated P91 weld metal
Slika 45: ACT-grafa deformacija – čas (a) in napetost – čas (b) pri 600 °C za po varjenju toplotno obdelan P 91-zvar

Table 4.1: Hardness results of P91/P92 materials after creep and after ACT
Tabela 4.1: Trdote jekel P91/P92 po preizkusu lezenja in po ACT

Material / sample / exposure	Micro-hardness HV 100G	
	initial	after exposure or testing
P91 component 1 – pipe / 3 years at 568 °C	n. a.	231
P91 component 1 – weld / 3 years at 568 °C	n. a.	258
P91 component 1 – bottle / 3 years at 568 °C	n. a.	243
P91 component 2 – antler / 9 years at 600 °C	n. a.	229
P91 component 2 – weld / 9 years at 600 °C	n. a.	208
P91 component 2 – stub / 9 years at 600 °C	n. a.	177
ACT – P91 standard weld metal with PWHT	285	223
ACT – P91 lean/soft weld metal low PWHT	298	193
ACT – P92 standard weld metal	294	240
ACT – P92 standard pipe	268	228

From the graph of **Figure 45a** for the zero-stress condition the progress of permanent extension can be read, while from graph of **Figure 45b** the decrease of tensile yield strength with progress of the creep can be observed as well as the change of elasticity modulus calculated. Micro-hardness measurements after the ACT show results comparable with these of multi-year creep exposed power generation components of the same grade material; some examples are given in **Table 4.1**.

4.3 Verification of results

The loss of steel's strength during creep is associated with transformation of its microstructure, which in the case of the Cr-Mo-V grade materials is due to precipitation of carbides and their coagulation and also to formation of intermetallic phases, so metallographic and microanalytical investigations are needed to confirm the reliability of the testing procedure.

In the case of the P91 steels and weld metals discussed here, their initial microstructures in the initial tempered state contain numerous fine and medium size carbide precipitates, relatively uniformly distributed in the ferritic matrix retaining its post-martensitic character, **Figure 46**. Such matrix, when seen in thin foil specimens in TEM, mostly consists of fine subgrains aligned in arrays of crystallographic orientations inherited from the former martensite microstructure, **Figure 47**. During exposure to creep conditions, in this initial microstructure further precipitation processes occur as well as

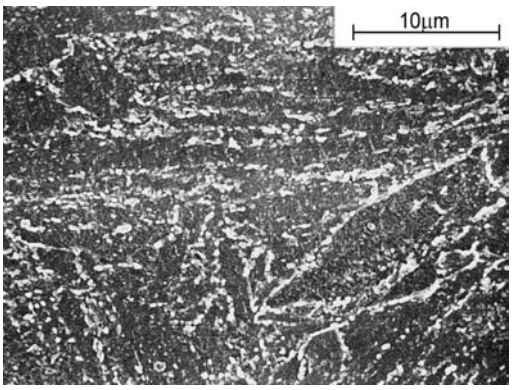

Figure 46: Tempered martensite microstructure of P91 steel; $FeCl_3$ etched, SEM image
Slika 46: Mikrostruktura iz popuščenega martenzita v jeklu P 91. Jedkano s $FeCl_3$; SEM-posnetek

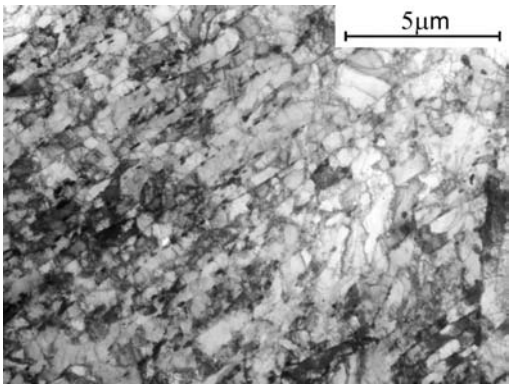

Figure 47: Arrays of subgrains with carbides in tempered martensite of P91 steel; thin foil specimen, TEM image
Slika 47: Področje podzrn s karbidi v popuščenem martenzitu v jeklu P 91, tanka folija; TEM-posnetek

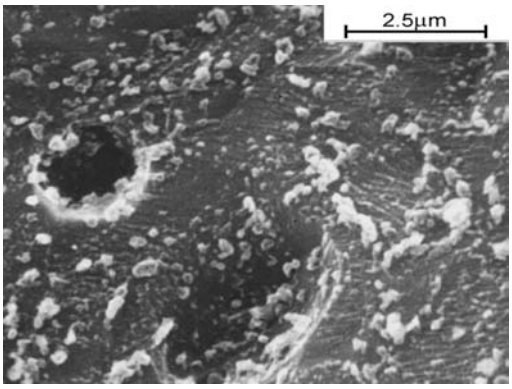

Figure 48: Fracture surface of ACT sample of P91 steel showing high density of carbides, $FeCl_3$ etched, SEM image

Slika 48: Prelomna površina ACT-preizkušanca iz jekla P 91, ki kaže veliko gostoto karbidov; jedkano s $FeCl_3$; SEM-posnetek

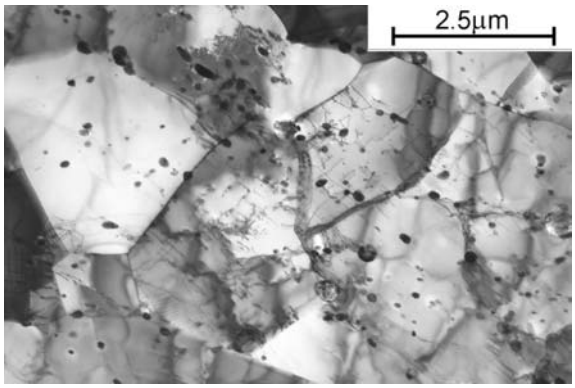

Figure 49: Recrystallised fine ferrite grains retaining oriented arrays of carbides in P91 sample after ACT at 600 °C; TEM, thin foil

Slika 49: Rekristalizirana fina feritna zrna, ki so obdržala orientirano porazdelitev karbidov v preizkušancu iz jekla P91 po ACT pri 600 °C, TEM, tanka folija

transformation of the existing carbides and their coagulation, in combination with recovery and recrystallisation of the matrix.

Accordingly, any reliable creep test should not generate microstructures much different from these taken from true services. The microstructures generated during the ACT appear to be a bit finer than after exposure to true creep while the precipitation of carbides especially at the surface of the internal crack seems to be somewhat more intensive, **Figure 48**. Nevertheless, on the fracture surfaces of the ACT samples the precipitated phases are identical with these after the long-term creep exposure and their content and chemical compositions do agree with the Thermocalc prediction of phases, which should be present at thermodynamic equilibrium [16]. On these fracture surfaces also traces of slip lines can be observed confirming that up to the onset of cracking the process is mainly controlled by dislocations glide and annihilation. Finally the microstructure after the ACT consists of well recrystallised grains with uniform distribution of spheroidal precipitates, mainly carbides, **Figure 49**.

5 CONCLUSIONS

1. Up-to-date physical simulation procedures allow studying materials behaviour at conditions very close to real industrial processing or applications.
2. The process parameters such like temperature, sense and amount of strain, strain rate as well as thermal gradients can be adequately reproduced and their values accurately recorded.
3. By means of physical simulation a large variety of microstructures and associated mechanical properties can be obtained and studied in a short time and for a tiny fraction of full-scale industrial experiments.
4. The materials behaviour data gained from physical simulation experiments can be further used in computer modeling and control of the industrial manufacturing processes.

6 REFERENCES

[1] E. F. Nippes & W. F. Savage; The Weldability of Ship Steel – A Study of the Effect of Travel Speed, Preheat Temperature and Arc Power Level on the Notch Toughness of the Weld Metal and the Heat-Affected Zone, Welding Journal 25 (**1946**), Res Suppl, p. 776s

[2] E. F. Nippes & W. F. Savage; *Tests of Specimens Simulating Weld Heat-Affected Zones*, Welding Journal 28 (**1949**), Res Suppl, p. 599s

[3] W. F. Savage et al; *An Investigation of the Hot Ductility of High Temperature Alloys*, Welding Journal 34 (**1955**), Res Suppl, p.183s

[4] Information on http://www.gleeble.com/

[5] S. T. Mandziej; *Physical Simulation of Welding*, in Proc ASM Intl Conf on Welding & Joining, Madrid, Spain, March 1997, p.253

[6] W. Lin, J. C. Lippold, W. A. Baeslack III; An Evaluation of Heat-Affected Zone Liquation Cracking Susceptibility, Part I: Development of a Method for Quantification', Welding Journal 72 (**1993**), Res Suppl, p.135

[7] C. D. Lundin et al; Hot ductility and hot cracking behavior of Modified 316 Stainless Steels designed for high temperature service, Welding Journal 72 (**1993**), Res Suppl, p.189

[8] *A Standard Procedure for Hot Cracking Test*, Dynamic Systems Inc, Poestenkill, NY, USA, 1995, IIW Doc. II-C-042A/95

[9] CEN ISO/TR 17641-3:2003, Destructive tests on welds in metallic materials – Hot cracking tests for weldments – Arc welding processes – Part 3: Externally loaded tests

[10] H. G. Suzuki, S. Nishimura, S. Yamaguchi; *Physical Simulation of the Continuous Casting of Steels*, in Proc Physical Simulation of Welding, Hot Forming and Continuous Casting, MTL 92-43(TR), CANMET, Canada, 1988, p. II-1

[11] L. Trebacz, R. Kuziak, M. Pietrzyk; *Numerical Model of the SICO Test*, Proc STEELSIM 2005, Brno CR, 2005, p.487

[12] S. T. Mandziej, J. D. Vosburgh, R. Kawalla, H.-G. Schoss; *Physical Simulation of Thin Slab Continuous Casting*, Materials Science Forum, Vols 539-547, 2007, p.4149

[13] B. Engel, M. Albedyhl, M. Brühl, Ch. Klinkenberg, H. Langner, H. Pircher, K. Wünnenberg; Stahl und Eisen 118 (**1998**) 5, 41

[14] H. S. Ferguson; *Fundamentals of Physical Simulation*, in Proc Intl Symposium on Physical Simulation, TU Delft 1992, p. 1

[15] S. T. Mandziej; *Low-Energy Dislocations and Ductility of Ferritic Steels*, in Fundamental Aspects of Dislocation Interactions, Materials Science & Engineering A, 164 (**1993**) 275

[16] S. T. Mandziej, A. Výrostková: Evolution of Cr-Mo-V weld metal microstructure during creep testing – Part 1: P91 material, Welding in the World, 52 (**2008**)1/2, 3